# Substantial climate response outside the target area in an idealized experiment of regional radiation management

**Sudhakar Dipu[1], Johannes Quaas[1], Martin Quaas[2], Wilfried Rickels[3], Johannes Mülmenstädt[1,a], Olivier Boucher[4]**

[1]Institute for Meteorology, Universität Leipzig, Germany
[2]German Centre for Integrative Biodiversity Research (iDiv) Halle-Jena-Leipzig / University of Leipzig, Germany
[3]Kiel Institute for the World Economy, Kiel, Germany
[4]Institut Pierre-Simon Laplace, Sorbonne Université / CNRS, Paris, France
[a]now at: Pacic Northwest National Laboratory, Richland, Washington, USA

**Key Points:**

- Regional radiation management (RRM), implemented in a coupled climate model in an ad hoc way over North America, results in a local cooling.
- However, the model also simulates substantial impacts outside the area of implementation with some regions experiencing a warming.
- Intermittent RRM, implemented only before and during predicted heatwaves, is successful in suppressing the heatwaves with little impact elsewhere, but only in a statistical sense.

Corresponding author: Sudhakar, dipu.sudhakar@uni-leipzig.de

**Abstract**

Radiation management (RM) has been proposed as a conceivable climate engineering (CE) intervention to mitigate global warming. In this study, we use a coupled climate model (MPI-ESM) with a very idealized setup to investigate the efficacy and risks of CE at a local scale in space and time (regional radiation management, RRM) assuming that cloud modification is technically possible. RM is implemented in the climate model by the brightening of low-level clouds (solar radiation management, SRM) and thinning of cirrus (terrestrial radiation management, TRM). The region chosen is North America, and we simulate a period of 30 years. The implemented sustained RM resulted in a net local radiative forcing of $-9.8\,\mathrm{Wm}^{-2}$ and a local cooling of $-0.8\,\mathrm{K}$. Surface temperature (SAT) extremes ($90^{th}$ and $10^{th}$ percentile) show negative anomalies in the target region. However, substantial climate impacts are also simulated outside the target area, with warming in the Arctic and pronounced precipitation change in the eastern Pacific. As a variant of RRM, a targeted intervention to suppress heat waves (HW) is investigated in further simulations by implementing intermittent cloud modification locally, prior to the simulated HW situations. The intermittent RRM results in most cases in a successful reduction of temperatures locally, with substantially smaller impacts outside the target area compared to the sustained RRM.

## 1 Introduction

Climate engineering (CE), also referred to as geoengineering, encompasses a set of technologies and methods to deliberately intervene in the climate system to counteract global warming (IPCC, 2013). The approach consists of either reducing the amount of solar radiation absorbed by the Earth, facilitating outgoing longwave radiation (radiation management, RM) or enhancing the net carbon sink from the atmosphere (carbon dioxide removal, CDR) in order to mitigate global warming (Boucher et al., 2014). In the past few years, CE garnered significant attention because if adequate measures to curb greenhouse gases in the atmosphere are not implemented rapidly, substantial warming over pre-industrial times can be expected (MacMartin et al., 2019; Betts et al., 2010; Battisti et al., 2009; M. MacCracken, 2009).

To tackle global warming, the Paris agreement in 2015 aims to limit the increase in global-mean near-surface temperature to below 2° C in comparison to pre-industrial times and to pursue efforts to limit the increase to below 1.5° C (Dimitrov, 2016; UNFCCC, 2015). Substantial reductions in greenhouse gas emissions as well as some amount of CDR are required to do so, but if such measures are insufficient or come too late, achieving these goals would imply some sort of RM. However, RM is expected to be imperfect (e.g., it may lead to overcooling of the tropics and undercooling of the poles) with potentially severe side effects (e.g., it modifies some precipitation patterns). Furthermore, it would not solve the issues of ocean acidification and ocean deoxygenation, and a putative early termination would cause rapid climate change (Keller et al., 2014; Tilmes et al., 2018). Thus, RM entails many social and ethical issues (Corner & Pidgeon, 2014) which to some extent also applies to research on RM (M. F. Quaas et al., 2017). However, without strong reduction in greenhouse gases and in the absence of CE methods (CDR and RM), anthropogenic climate change could result devastating consequences with 3–4 ° C or more temperature rise by the end of the $21^{st}$ century (Wigley, 2006; Wigley & Raper, 2001; Rahm, 2018; Cox et al., 2018), which would also generate significant social and ethical concerns (Preston, 2013). In this context, RM might be proposed to "shave off" the peak of climate warming due to anthropogenic greenhouse gases, before the $CO_2$ removal and greenhouse gases mitigations become sufficient (Tilmes et al., 2009; Kravitz et al., 2011; A. C. Jones et al., 2017; Tilmes et al., 2018; MacMartin et al., 2019). J. Quaas et al. (2016) argued that local implementation of RM seems more likely than a global implementation. One key reason for this is that different countries or different regions of the world have different preferences with regard to climate change. A regional implementation might also occur as an interim step before global action is taken (M. C. MacCracken, 2016). Various climate projections with RM

techniques propose that the radiative forcing (RF), a measure of energy budget perturbation, is substantially localized to the region of implementation (Stjern et al., 2018; Aswathy et al., 2015; A. Jones et al., 2009; Mitchell & Finnegan, 2009). Local mitigation seems a necessary but not a sufficient condition for regional RM (RRM) to be of interest, because the climate effects may extend outside the region. The extended climate effect may be beneficial or detrimental while the pattern of influence strongly depends on the region of RRM implementation (Tilmes et al., 2018; A. Jones et al., 2009). By using an example, here we demonstrate that RRM may lead to non-local responses which are modulated by the atmospheric circulation, and subsequently we demonstrate that limiting RRM also in time substantially reduces these side-effects.

Proposed RM management schemes involve reflecting solar radiation away from the Earth's atmosphere [solar radiation management, SRM; Barker et al. (2007)], and increasing the outgoing longwave radiation at the top of the atmosphere [terrestrial radiation management, TRM; Mitchell and Finnegan (2009); Mitchell et al. (2008)]. SRM techniques aim to manipulate the global temperature by increasing the albedo of the atmosphere. Among CE options, some SRM techniques are potentially comparatively inexpensive, technologically feasible, and would lead to a rapid response of the climate system (Robock et al., 2008; Matthews & Caldeira, 2007). SRM includes methods such as the sulphate aerosol injection into the stratosphere, or increasing the reflectivity of low-level clouds, and possibly also their lifetime, by adding aerosols to the troposphere (Carr et al., 2013; Moreno-Cruz et al., 2012; D. Keith et al., 2010; Tilmes et al., 2009; Heckendorn et al., 2009; Robock et al., 2008; Wigley, 2006). The response of climate to stratospheric aerosol injection (SAI) has been investigated in many modeling studies [e.g., Tilmes et al. (2018); A. Jones et al. (2009); MacMartin et al. (2017); MacMartin and Kravitz (2019); Kravitz et al. (2011); Tilmes et al. (2009); Heckendorn et al. (2009); A. Jones et al. (2010); Aswathy et al. (2015)]. These suggest that SAI could possibly stabilize the global mean surface temperature. The problem that equatorial injection of stratospheric aerosols leads to an overcooling of the tropics relative to the higher latitudes can possibly be overcome by optimized injection at multiple locations (MacMartin et al., 2017). SAI focusing on the polar regions can even have a larger influence in high compared to low latitudes (M. C. MacCracken et al., 2013; Caldeira & Wood, 2008). Besides the cooling, large-scale SAI could lead to consequences such as a shift in precipitation patterns (Haywood et al., 2013; A. C. Jones et al., 2017), reduction in monsoon precipitation (Tilmes et al., 2013), and unmitigated characteristics of temperature and precipitation extremes (Aswathy et al., 2015). Further, SAI would also delay the recovery of the ozone layer and enhance environmental risks (D. Keith et al., 2010; Heckendorn et al., 2009; Tilmes et al., 2009; Crutzen, 2006). However, MacMartin et al. (2019) suggested that for a limited deployment of SAI, the projected change in surface temperature, precipitation, and precipitation minus evaporation are typically smaller than natural variability.

In addition to SAI, marine cloud brightening (MCB) has been proposed as a possible SRM approach (Wood & Ackerman, 2013; Latham et al., 2012; Latham, 1990). The suggestion is to modify low-level marine clouds by injecting aerosols into the marine boundary layer and so increase cloud albedo. Such modification would produce a negative RF, which implies a cooling of surface temperature (Twomey, 1977). This approach is most effective in relatively clean areas (Wood & Ackerman, 2013). Ship tracks and the impact of volcanic eruptions on marine clouds provide observational evidence of the cloud albedo effect (Robock et al., 2013). Several modeling studies reported that, in principle, MCB has the potential to cool the Earth substantially (A. Jones et al., 2009; Robock et al., 2008; Latham, 2002). Aswathy et al. (2015) examined multi-model simulations of SAI and MCB. They demonstrated that both methods offset the effect of global warming, with more cooling in lower latitudes and residual warming in the Arctic. Aswathy et al. (2015) further discussed the discrepancy in extreme temperature and precipitation for the two different CE schemes (SAI and MCB). Finally, some studies suggest that sudden termination of SRM may cause an acceleration of global warming, which is another important risk of SRM (Kosugi, 2013;

Brovkin et al., 2009). However, the sudden termination of strong SRM implementation might not be the most realistic scenario (Parker & Irvine, 2018).

Another way of manipulating the net radiative flux of the planet could be through the thinning of high-level cirrus clouds (deliberate reduction of the cloud cover and optical thickness) (Duan et al., 2018; Gruber et al., 2019). Cirrus thinning reduces the absorption of longwave radiation emitted from the Earth's surface and the atmosphere beneath it, which results in a cooling (Mitchell & Finnegan, 2009; Muri et al., 2014; Storelvmo et al., 2014). However, altitude, optical depth, cloud microphysics, and reflectivity of sunlight play a pivotal role in cirrus radiative effects (Campbell et al., 2018; Masunaga & Bony, 2018). Storelvmo et al. (2013) have tested the cirrus thinning hypothesis in a global climate model and found that it has the potential to counteract anthropogenic global warming. For cirrus cloud modification, a preliminary estimate of the potential global change in cloud radiative effect of up to $-2.8\,\mathrm{Wm}^{-2}$ has been reported, which could almost offset the RF due to $CO_2$ doubling (Mitchell & Finnegan, 2009). However, the effect of this magnitude is quite theoretical. It could be a complementary measure to SAI if implemented regionally over polar regions in the winter season. However, cirrus thinning in the polar regions would modify the equator to the pole temperature gradient (Tilmes et al., 2014; M. C. MacCracken et al., 2013; M. C. MacCracken, 2016).

Previous studies (some of which are discussed above) have provided insight into various RM methods, their efficacy, and risks. Studies that have examined the possibility of RRM through the dimming of solar radiation were limited to the Arctic (Tilmes et al., 2014; Caldeira & Wood, 2008). Outside the Arctic, RRM raises critical questions if different countries and regions of the world have a different perspective on climate change and/or CE. Nevertheless, it is essential to identify the regional response to climate change (Ge et al., 2019).

In this context, J. Quaas et al. (2016) pointed out that RRM could further be limited by implementing them only "on demand" to target certain climate extreme events, in particular, heat waves (HW). From observations and model projections, it is evident that, with climate change, the present-day HWs are likely to become more frequent, intense, and longer with substantial impact on human health (Herring et al., 2014; Wolf et al., 2010; Sun et al., 2014; G. S. Jones et al., 2008; Meehl & Tebaldi, 2004). In recent decades, climate models are increasingly able to reproduce climate extremes as well as their response to forcings (Sillmann et al., 2013). Wang et al. (2013) simulated the effect of RRM by increasing the surface albedo of urban roofs, which allows for some HW suppression. This implies that mitigation measures such as RRM could potentially reduce the impact of the HW and its consequences.

In RM research, deployment scenarios play a pivotal role in assessing efficacy and risks. Most of the RM scenarios are aiming to offset the global mean temperature rise. However, the recent emphasis is on moderate and restrained deployment (D. W. Keith & MacMartin, 2015; Irvine et al., 2019; Sugiyama et al., 2018). In this study, we have considered the scenario of a regional intervention (local mitigation or RRM) in a mid-latitude region, using a state-of-the-art climate model under the assumption that cloud modification is technically possible. This study investigates the efficacy and impacts of regional mitigation by sustained RM, the HW suppression by intermittent RM, and its impacts outside the target region. A brief description of the model, the experimental design, and methodology are provided in section 2. Section 3 discusses the response of temperature and precipitation to RRM. In a further step, we investigate a setup in which only suppresses the HW, rather than sustained RRM, is implemented. Finally, concluding remarks are given in section 4.

# 2 Data and Methodology

## 2.1 Model description

The simulations on which this study relies have been performed with a coupled atmosphere-ocean-land surface model, the Max Planck Institute Earth system model (MPI ESM) (Giorgetta et al., 2013). It consists of the atmospheric component ECHAM6 (Stevens et al., 2013) with T63L47 spectral resolution (about 1.8° in the horizontal, uppermost of the 47 levels at 0.01 hPa), and the ocean component Max Planck Institute Ocean Model (MPIOM) (Jungclaus et al., 2013), which applies an idealized control mapping grid of about 1.5 ° with 40 levels. The atmospheric composition, as well as other boundary conditions, are prescribed at pre-industrial conditions. The simulations are initialized with existing pre-industrial equilibrium simulation and are run for 30 years. The two reasons to choose the pre-industrial climate are (i) the practical one that a balanced equilibrium atmosphere-ocean state is available and (ii) that the analysis is facilitated since the only transient perturbation is the imposed one. Although we agree that RRM would be more realistically tested in a future scenario, it is very unlikely to change the results. The key mechanisms documented in our study would be equally present no matter what the baseline climate is. Furthermore, the choice of the scenario would be arbitrary.

## 2.2 Experimental design

The aim of these experiments is an analysis of RRM, targeting a continental area encompassing 32.5° N to 47.5° N and 112.0° W to 92.0° W (Supplementary Fig. S1). North America is chosen somewhat arbitrarily, but there is one key argument: it is a mid-latitude region where no directly neighboring countries are located in the zonal direction, so that comparatively little effects of RRM in other countries may be expected. The exact location of the box within North America is arbitrary and again idealized.

Three types of model experiments are performed. First, a control simulation is performed without any cloud modification. A second type of simulations is performed where an idealized regional cloud modification (see section 2.2.1) is sustained throughout the simulation over the targeted region. This second type of simulations is referred to as the "sustained mitigation" experiment and is evaluated against the control simulation. A third type of simulations is also performed where cloud modification is implemented only for the periods when in the control simulation there is a HW in the region of interest. This third type of simulations is used to evaluate the impact of "intermittent mitigation". In this case, the simulation is stopped a little after a HW is detected over the target area, it is then rewound and restarted with the cloud modification applied for a short period before, during and after the HW is simulated in the initial simulation. The scenario is meant to represent the fact that RRM is triggered then a HW is forecast by numerical weather prediction. We define HW conditions as periods when the area mean of daily maximum temperature within the target region exceeds a threshold value, selected here as 32° C, for at least three consecutive days. In such an event, RRM is implemented starting 10 days preceding the HW (Supplementary Fig. S2). This 10-day period is a lead time at which numerical weather prediction is reliable, and long enough to allow the surface temperature to respond to the cloud modification. RRM is then sustained until one week after the end of the HW in the original simulation. The simulation with HW suppression then becomes the main simulation and is continued (consistent with the scenario, Supplementary Fig. S2). If multiple HW episode occurs within a period (less than 10 days between the HWs), then such events are combined and treated as a long single HW condition. In this third type of simulations, the periods with HW suppressions are evaluated against the corresponding periods without HW suppression that were simulated before the simulation is rewound to apply the cloud modification.

To reduce the uncertainty associated with the simulated interannual variability, a six-member ensemble is performed and analyzed. The ensemble members are performed only

for sustained and intermittent experiments. For the sustained experiment, each ensemble member uses the same external forcing besides a small perturbation in the atmospheric initial conditions. Thus the statistics are performed on a period of $6 \times 30$ years $= 180$ years. For the intermittent experiment, the perturbation is applied only during the HW suppression period (Supplementary Fig. S2).

The cloud modification influences the Earth's climate by perturbing the Earth's energy budget at the top of the atmosphere, which referred to as the effective radiative forcing (ERF). It is defined as the difference between the net radiative flux at the top of the atmosphere for the experiment (with RRM) and the control simulation (without RRM). However, since the integration time is short enough, there is still the bulk of the top-of-atmosphere radiation imbalance that makes up the ERF. To compute statistical significance levels, a Welch's unpaired $t$-test is used (Welch, 1947; Boneau, 1960). In both experiments, a set of climate extremes is identified with the upper and lower end of the distribution of meteorological variables, for instance, top and bottom deciles ($90^{th}$ and $10^{th}$ percentiles, respectively) of surface temperature (Aswathy et al., 2015). In the following text, the changes in temperature, precipitation, wind etc are the mean changes over 30 years (experiment - control) and local/locally denote the experiment region.

#### *2.2.1 Cloud modification*

Cloud optical properties have a profound impact on the global radiative effect (Twomey, 1977). Optically thick boundary layer clouds exert a negative radiative effect, by reflecting solar radiation and little greenhouse effect (McComiskey & Feingold, 2008; Twomey, 1977), whereas optically thin high-level clouds have a positive radiative effect by blocking the terrestrial radiation (Mitchell & Finnegan, 2009). Here the cloud modification is implemented as an alteration to both types of clouds by multiplying the liquid cloud water content $q_{\mathrm{l}}$ by a factor of 10 and multiplying the cloud ice content $q_{\mathrm{i}}$ by a factor of 0.1 in the model, specifically over the target region ($q_{\mathrm{l}}$ and $q_{\mathrm{i}}$ are local variables in the radiation module). This modification is made at every timestep because the change does not affect processes other than the radiation. The change intentionally is large to obtain a climate signal. This effectively assumes that technologically, such a cloud modification is feasible, and neglects possible implications of the specific technology. Since the above modification will work only if $q_{\mathrm{l}} > 0$ and/or $q_{\mathrm{i}} > 0$, the magnitude of the cloud modification strongly depends on the presence and thermodynamic phase of cloud layers in the atmospheric column.

## 3 Results

### 3.1 Sustained mitigation

The implemented RM in the climate model (see section 2.2.1) increases the reflection of solar radiation by liquid-water clouds (negative radiative effect) and reduces the cirrus greenhouse effect by allowing more terrestrial radiation to escape to space (i.e. to reduce the absorption of longwave radiation emitted from the Earth's surface and the atmosphere beneath; negative radiative effect). Both lead to a negative local RF. Fig. 1a shows the diagnosed effective RF (ERF) at the top of the atmosphere, which yields a magnitude of $-9.8 \pm 5\,\mathrm{Wm}^{-2}$ over the target/experiment region. The negative forcing leads to a cooling of the near surface air temperature (SAT) with a mean of $-0.8 \pm 0.7\,\mathrm{K}$ in the target region (Fig. 1b). The radiative effect of RRM was further untangled by a separate assessment of the two different cloud modifications (thickening of liquid clouds, mainly in the solar spectrum; and thinning of ice clouds, mainly in the terrestrial spectrum) to find that the thickening of the liquid cloud contributes 54% to the total regional forcing, with the remainder from the thinning of ice clouds (Figure not shown). An important result of the simulation is that besides this intended effect, also a high latitude warming is evident over the Alaskan region, which is statistically significant at 90% confidence level.

From the geographical distribution, the main contributor to the high latitude warming is the anomalous warming simulated to the northwest of the experimental region (Alaskan region). As a consequence of the local cooling, there is a weakening of surface westerly wind flow resulting in an anomalous north to northwesterly flow in the western Pacific between 30° N to 60° N and 120° W to 180° W (Fig. 2a). This anomalous flow favors incursions of warm air masses from mid-latitude to high latitudes. Associated with RRM and high latitude warming, a significant change in circulation, and geopotential height are also noted at higher altitudes. The positive anomalies of geopotential and temperature at 500 hPa result in an anomalous anticyclonic circulation over the warm region and a cyclonic circulation over the target region (Fig. 2b). These circulations result in the convergence of warm air (anticyclonic) and divergence of cold air (cyclonic) above the respective regions. This teleconnection is analogous to the finding of Kug et al. (2015), although it suggests an influence of Arctic warming on North American cold winters, which is the opposite interpretation of causation. Note that in our simulations, the causation is imposed by construction. There is some seasonality to the results. The colder winters in North America in response to RRM are the major contributor to anomalous Arctic warming. The anomalous cold winter due to RRM cooling provides a favorable condition for the Arctic warming through the poleward intrusion of warm air from mid-latitudes (Fig. 2). Furthermore, the sea ice area fraction shows a decrease over the Alaskan region, which is associated with sustained warming of the Alaskan region due to the North American RRM. In turn, in the polar region, the sea ice fraction shows an increase (Fig. S3a). The change in sea ice fraction could be related to the seasonality in ERF. It has both contributions from ice and liquid cloud modifications (Figure not shown), with a relatively significant negative ERF in the winter season, which leads to seasonality in SAT as well. The seasonality in the RRM induced SAT anomaly (Fig. S4) leads to an imbalance between summer ice melt and winter ice growth (Fig. S3b & c), which accelerates sea ice loss around the Alaskan region, especially in the Bering Sea and the Sea of Okhotsk.

An even more pronounced effect outside the targeted area is found when considering SAT extremes as defined by the top and bottom deciles of the temporal distribution at each grid point (Fig. 3). The geographical distribution of change in the top decile of the SAT shows a cooling of the temperatures over the experiment region and exhibits a spatial pattern that is similar to the mean SAT change pattern, with local cooling. However, in the bottom decile of the SAT distribution, along with the expected reduction over the target area, significant warming is simulated over much of the high latitudes (between 60° N and 90° N) of the Northern Hemisphere, with a statistical significance at a confidence level of 90%. Indeed in the bottom decile of the SAT, the warmings are statistically significant, especially over the Arctic, emphasizing the non-local influence of RRM, attributable to the teleconnection mechanism discussed above. The signal in the bottom decile is noisy, however, with some – less significant – negative anomalies in the high latitudes as well.

For precipitation, the RRM simulation shows a slight local increase by on average $0.02\,\mathrm{mm\,day^{-1}}$, despite the cooling (Fig. 4). However, pronounced alterations of precipitation are also simulated elsewhere across the globe, especially in the eastern Pacific region. The large positive precipitation anomalies in the eastern Pacific warm pool region are related to an RRM teleconnection. It can be delineated from the time series of: (1) standardized SAT anomaly in the RRM region, (2) standardized sea surface temperature (SST) anomaly in the Niño3.4 region (5° S to 5° N, 120° W to 170° W), and (3) standardized total precipitation anomaly in the eastern Pacific (0° S to 10° S, 148° W to 180° W). Fig. 5 shows the relationship between SAT, SST, and precipitation, each in the distinct regions. Although RRM results in a local reduction in temperature on average, there exists variability in the local cooling. The time series illustrates a negative correlation between SAT in the RRM region with Niño3.4 SST and precipitation. The negative correlation implies that the intensity of the local RRM cooling has a significant teleconnection to the Pacific warming/cooling which leads to positive/negative precipitation anomalies.

The teleconnection is further investigated by analyzing the composite anomalies of SAT, precipitation, and wind vector when (1) the standardized SAT anomaly is greater than −1.0 K, and (2) the standardized SAT anomaly is less than −1.0 K in the RRM region. Fig. 6 shows the co-variability of the local SAT variability with global climate. During relatively small cooling (SAT $> -1.0$ K) conditions, the climate variability is analogous to La Niña conditions with a cool Pacific Ocean SST and a dry western Pacific (Fig. 6a). It is associated with a divergent wind vector anomaly in the eastern Pacific along with northerly wind flow, and an anticyclonic circulation over the north-central Pacific, which relates to the warm SAT anomalies. However, periods of strong cooling in the RRM region (SAT anomaly $< -1.0$ K) relate to climate variability similar to El Niño conditions (Fig. 6b). During the strong RRM cooling episodes (time periods below the dotted line in Fig. 5), relatively strong cooling is simulated over North America and East Asia, while significant warming is simulated for the tropics (central Pacific). In the tropics, SAT patterns reflect the SST pattern. Positive SAT anomalies are also simulated for the high latitudes over the north-east Pacific and extend well into the Alaskan region. As a consequence of significant local cooling, the surface westerly wind weakens and results in an anomalous northerly flow, which contributes to the anomalous warming in the Alaskan region. Additionally, it results in an equatorial wind convergence and enhances the convection in the west Pacific, thus the precipitation (Fig. 6b).

Graf and Davide (2012) demonstrated teleconnections between El Niño and Atlantic / European regional climates, which involve a dynamic coupling of the troposphere with the stratosphere. A similar coupling mechanism is also noticeable when assessing the position of the sub-tropical jet streams in the two simulations (Fig. 6). Situations with relatively limited RRM local cooling show little change in the position of the jet (Fig. 6a). However, intense local SAT change is correlated with a shift of the jet core towards the Equator over the north Pacific (Fig. 6a). This dynamical coupling mechanism can be further explained by upper tropospheric circulations (Fig. S5a & b). In the Northern Hemisphere mid-latitudes, the stream function anomalies are similar to the geopotential height anomalies in terms of their pattern, with anti-cyclonic and cyclonic circulation anomalies in the positive and negative stream function positions, respectively. During the time of relatively little RRM cooling (SAT anomaly $> -1.0$ K), a pronounced chain of significant positive stream function anomalies, as well as anti-cyclonic circulations in the Northern Hemisphere, is simulated. Over the western Pacific, upper-level convergence can be noticed (Fig. 6c). The upper-level convergence and lower-level divergence explain the negative precipitation anomalies (Fig. 6a & Fig. S5a). On the other hand, composite anomalies for relatively strong RRM cooling (SAT anomaly $< -1.0$ K) relate to a pronounced chain of significant negative stream function anomalies with cyclonic conditions in the Northern Hemisphere with negative geopotential height field. It appears that the strong low-level convergence and upper-level divergence over the western Pacific lead to pronounced precipitation in this region (Fig. 6b & Fig. S5b). These anomalies are associated with the intensity of RRM cooling, and the proposed link mechanism is the dynamic coupling of the troposphere with the upper troposphere.

As discussed earlier the chosen location for RRM is somewhat arbitrary and it could be applied over other regions as well. Additional experiments with RRM implemented over the central European region indicate that our key conclusion holds. Assuming that clouds can be modified, a regional ERF and thus regional temperature change can be achieved. Furthermore, remote effects outside the target region are also visible (not discussed here).

### 3.2 Intermittent mitigation

As discussed above, sustained limited-area climate engineering can result in substantial climate alterations in other regions. In light of this, RRM can be less attractive than it initially might seem. Consequently, we now investigate to which extent RRM, if implemented in a temporally intermittent (non-continuous) way, may be useful to suppress harmful extreme weather conditions – here HWs are selected – without causing substantial

impact outside the targeted region. Sixteen HWs occur during the three decades of our "intermittent mitigation" simulation (Supplementary material, Table T1).

Fig. 7 illustrates the evaluation of a case with ensemble mean HW suppression against the corresponding period without HW suppression. The RRM deployed HW suppression leads to local cooling and retains the temperature below the HW threshold temperature of 32° C. We have selected a case for Fig. 7, that shows a clear avoidance of the HW, whereas in other cases HW mitigation is not as efficient (Supplementary Fig. S6). In most cases, the mitigation acts to reduce the HW, even if it does not completely avoid exceeding the threshold temperature. The reason is that the magnitude of mitigation strongly depends on the presence of suitable clouds, where the HW with clear skies implies no alteration is introduced. The time average (30 years) of the ERF (Fig. 8b) is much smaller than in the case of the sustained RRM. Similarly, the SAT changes are also much smaller (Fig. 8b). However, a significantly positive SAT anomaly is simulated to the North of the RRM region. Likewise, the temperature extremes, top and bottom deciles of SAT distribution, also reveal a less significant impact outside the target region (Fig. 8c & d). However, the bottom decile exhibits an enhanced cooling in the north-eastern part and warming to the north of the RRM region.

These results suggest that intermittent local HW suppression could have potential – though not systematic– benefits on human and ecosystem health (Herring et al., 2014) with smaller side effects than permanent HW suppression. However, we also underline that it is not possible to intervene, even intermittently, without any consequences elsewhere at all.

## 4 Conclusions

It has been suggested that, rather than global CE implementation, RRM might be more plausible from a geopolitical viewpoint as it may be considered by some countries or groups of countries who have their own climate preferences (J. Quaas et al., 2016). In this study, we have used a coupled climate model, the MPI-ESM, to assess the implementation of RRM. This implementation considers an idealized alteration of clouds in the model. For this, we have employed a modification of cloud properties (only in the radiation module) by scaling both liquid and ice clouds to generate optically thick boundary layer clouds and thinner high clouds, both generating a negative RF. The radiative perturbation resulting from this is quite large and no known technology could achieve it. However, the experiment is useful in that it provides an estimate for the size of the outcome to be expected for a large perturbation. Any smaller perturbation is expected to have a smaller outcome as well as smaller side effects. Our study addressed the impact of RRM and its consequences. We have chosen here the example of RRM implemented over North America. Local ERF is $-9.8\,\mathrm{Wm}^{-2}$ with a local cooling of $-0.8\,\mathrm{K}$. However, substantial effects outside the target region are also noticed. Especially over the Alaskan region, substantial warming is simulated and can be traced to a weakening of surface westerly wind flow. This warming is enhanced by north and northwesterly flow at the surface, along with 500 hPa anti-cyclonic flow over Alaska and a cyclonic circulation over the target region.

A slight increase in the local precipitation of $0.02\,\mathrm{mm\,day}^{-1}$ is noticed, despite the local cooling. Pronounced precipitation changes are also simulated outside the target area, especially in the eastern Pacific. Our analysis revealed that the relatively strong local RRM cooling results in a weakening of surface westerly wind and leads to equatorial wind convergence over the central Pacific. This, in turn, leads to a warm Pacific Ocean SST anomaly and enhances the precipitation in the eastern Pacific. The upper-level (200 hPa) anomalies for stream function, wind vector, and geopotential height also reveal the dynamic coupling of the troposphere with the stratosphere.

In a second step, we have studied the feasibility of deploying RRM to mitigate specific harmful weather events that may occur more intensely and more frequently in a warming

climate. We chose to target HWs and did so by implementing temporally intermittent RRM, which would presumably lead to less inadvertent effects. The idealized HW suppression scenario assumes accurate predictability of HWs. The results suggest that HWs are mitigated locally with the intermittent implementation of cloud modification by retaining the SAT below the threshold of 32° C in some cases. Further, the long term effect of HW suppression shows that the intermittent RRM results in much smaller time-average forcing, surface tempeature, or precpitation changes compared to the sustained RRM. However, some regional changes outside the target region are still simulated.

This study is illustrative of what RRM may look like and what its consequences could be, which relies on a hypothetical scenario (J. Quaas et al., 2016). Idealized studies like this one are crucial to quantify the regional effect of CE and its consequences on neighboring or more remote regions. Most of the RRM studies have focused so far on the polar (M. C. MacCracken, 2016; Tilmes et al., 2014; M. C. MacCracken et al., 2013; Caldeira & Wood, 2008) and oceanic regions (Wood & Ackerman, 2013; Latham et al., 2012; A. Jones et al., 2009), while RRM studies focusing on continental areas are sparse. Such studies are relevant because different countries and regions of the world have different perspectives on climate change and/or CE. Although it is idealized, our study shows that it would not be appropriate to implement RRM unilaterally, if such RRM technologies become available in the future.

## Acknowledgments

The MPI-ESM is developed by the Max Planck Institute for Meteorology, and was run on the facilities of the German Climate Computing Centre (Deutsches Klimarechenzentrum, DKRZ). This study was funded by the German Research Foundation (Deutsche Forschungsgemeinschaft, DFG) within the Priority Programme SPP 1689 "Climate Engineering - Risks, Challenges, Opportunities?" project LEAC-II (GZ QU 311/10-2 and QU 357/3-2). The data that support the findings of this study are available at http://doi.org/10.5281/zenodo.3956312. We thank an anonymous reviewer for very constructive remarks.

## References

Aswathy, V. N., Boucher, O., Quaas, M., Niemeier, U., Muri, H., Mülmenstädt, J., & Quaas, J. (2015). Climate extremes in multi-model simulations of stratospheric aerosol and marine cloud brightening climate engineering. *Atmos. Chem. Phys.*, *15*(16), 9593–9610. doi: 10.5194/acp-15-9593-2015

Barker, T., Bashmakov, I., Bernstein, L., Bogner, J., Bosch, P., Dave, R., ... Zhou, D. (2007). *Technical summary. in climate change 2007: Mitigation* (B. Metz, O. Davidson, P. Bosch, R. Dave, & L. Meyer, Eds.). Cambridge University Press.

Battisti, D., Blackstock, J. J., Caldeira, K., Eardley, D. E., Katz, J. I., Keith, D. W., ... Socolow, R. H. (2009). Climate engineering responses to climate emergencies. *IOP Conference Series: Earth and Environmental Science*, *6*(45), 452015. doi: 10.1088/1755-1307/6/45/452015

Betts, R. A., Collins, M., Hemming, D. L., Jones, C. D., Lowe, J. A., & Sanderson, M. G. (2010). When could global warming reach 4°C. *Phil. Trans. R. Soc. A*, *369*(1934), 67–84. doi: 10.1098/rsta.2010.0292

Boneau, C. A. (1960). The effects of violations of assumptions underlying the t test. *Psychol. Bull.*, *57*(1), 49-64. doi: http://dx.doi.org/10.1037/h0041412

Boucher, O., Forster, P. M., Gruber, N., Ha-Duong, M., Lawrence, M. G., Lenton, T. M., ... Vaughan, N. E. (2014). Rethinking climate engineering categorization in the context of climate change mitigation and adaptation. *WIREs Clim. Change*, *5*(1), 23–35. doi: 10.1002/wcc.261

Brovkin, V., Petoukhov, V., Claussen, M., Bauer, E., Archer, D., & Jaeger, C. (2009). Geoengineering climate by stratospheric sulfur injections: Earth system vulnerability to technological failure. *Clim. Chang.*, *92*(3), 243–259. doi: 10.1007/s10584-008-9490

-1

Caldeira, K., & Wood, L. (2008). Global and Arctic climate engineering: numerical model studies. *Phil. Trans. R. Soc. A*, *366*(1882), 4039–4056. doi: 10.1098/rsta.2008.0132

Campbell, J. R., Peterson, D. A., Marquis, J. W., Fochesatto, G. J., Vaughan, M. A., Stewart, S. A., ... Welton, E. J. (2018). Unusually Deep Wintertime Cirrus Clouds Observed over the Alaskan Subarctic. *Bull. Am. Meteorol. Soc.*, *99*(1), 27-32. doi: 10.1175/BAMS-D-17-0084.1

Carr, W. A., Preston, C. J., Yung, L., Szerszynski, B., Keith, D. W., & Mercer, A. M. (2013). Public engagement on solar radiation management and why it needs to happen now. *Clim. Chang.*, *121*(3), 567–577. doi: 10.1007/s10584-013-0763-y

Corner, A., & Pidgeon, N. (2014). Geoengineering, climate change scepticism and the 'moral hazard' argument: an experimental study of UK public perceptions. *Phil. Trans. R. Soc. A*, *372*(2031). doi: 10.1098/rsta.2014.0063

Cox, P., Huntingford, C., & Williamson, M. (2018). Emergent constraint on equilibrium climate sensitivity from global temperature variability. *Nature*, *553*, 319-322.

Crutzen, P. J. (2006). Albedo enhancement by stratospheric sulfur injections: A contribution to resolve a policy dilemma? *Clim. Chang.*, *77*(3), 211. doi: 10.1007/s10584-006-9101-y

Dimitrov, R. (2016). The Paris Agreement on climate change: Behind closed doors. *Global Environ. Polit.*, *16(3)*, 1-11.

Duan, L., Cao, L., Bala, G., & Caldeira, K. (2018). Comparison of the fast and slow climate response to three radiation management geoengineering schemes. *J. Geophys. Res.*, *123*(21), 11,980-12,001. doi: 10.1029/2018JD029034

Ge, F., Zhu, S., Peng, T., Zhao, Y., Sielmann, F., Fraedrich, K., ... Ji, L. (2019). Risks of precipitation extremes over southeast asia: does 1.5°C or 2°C global warming make a difference? *Environ. Res. Lett.*, *14*(4), 044015. doi: 10.1088/1748-9326/aaff7e

Giorgetta, M. A., Jungclaus, J., Reick, C. H., Legutke, S., Bader, J., Böttinger, M., ... Stevens, B. (2013). Climate and carbon cycle changes from 1850 to 2100 in MPI-ESM simulations for the Coupled Model Intercomparison Project phase 5. *J. Adv. Model. Earth Syst.*, *5*(3), 572-597. doi: 10.1002/jame.20038

Graf, H., & Davide, Z. (2012). Central pacific El Niño, "the subtropical bridge", and Eurasian climate. *J. Geophys. Res.*, *117*(D1). doi: 10.1029/2011JD016493

Gruber, S., Blahak, U., Haenel, F., Kottmeier, C., Leisner, T., Muskatel, H., ... Vogel, B. (2019). A process study on thinning of Arctic winter cirrus clouds with high-resolution ICON-ART simulations. *J. Geophys. Res.*, *124*(58605888). doi: 10.1029/2018JD029815

Hastings, D. A., Dunbar, P. K., Elphingstone, G. M., Bootz, M., Murakami, H., Maruyama, H., ... MacDonald, J. S. (1999). The Global Land One-kilometer Base Elevation (GLOBE) Digital Elevation Model, Version 1.0. *National Oceanic and Atmospheric Administration, National Geophysical Data Center, 325 Broadway, Boulder, Colorado 80305-3328*.

Haywood, J. M., Jones, A., Bellouin, N., & Stephenson, D. (2013). Asymmetric forcing from stratospheric aerosols impacts Sahelian rainfall. *Nature Clim. Change*, *3*, 660-665. doi: https://doi.org/10.1038/nclimate1857

Heckendorn, P., Weisenstein, D., Fueglistaler, S., Luo, B. P., Rozanov, E., Schraner, M., ... Peter, T. (2009). The impact of geoengineering aerosols on stratospheric temperature and ozone. *Environ. Res. Lett.*, *4*(4), 045108.

Herring, S. C., Hoerling, M. P., Peterson, T. C., & Stott, P. A. (2014). Explaining extreme events of 2013 from a climate perspective. *Bull. Amer. Meteor. Soc.*, *95*(9), S1-S104. doi: 10.1175/1520-0477-95.9.S1.1

IPCC, . (2013). Climate Change 2013: The Physical Science Basis. Contribution of Working Group I to the Fifth Assessment Report of the Intergovernmental Panel on Climate Change. *Cambridge University Press, Cambridge, United Kingdom and New York, NY, USA*, 1535 pp. doi: 10.1017/CBO9781107415324

Irvine, P., Emanuel, K., He, J., Horowitz, L. W., Vecchi, G., & Keith, D. (2019). Halving

warming with idealized solar geoengineering moderates key climate hazards. *Nature Clim. Change*, *9*(4), 295-299. doi: 10.1038/s41558-019-0398-8

Jones, A., Haywood, J., & Boucher, O. (2009). Climate impacts of geoengineering marine stratocumulus clouds. *J. Geophys. Res.*, *114*(D10). (D10106) doi: 10.1029/2008JD011450

Jones, A., J, H., Olivier, B., Ben, K., & Robock, A. (2010). Geoengineering by stratospheric $SO_2$ injection: results from the Met Office HadGEM2 climate model and comparison with the Goddard Institute for Space Studies ModelE. *Atmos. Chem. Phys.*, *10*(13), 5999-6006. doi: 10.5194/acp-10-5999-2010

Jones, A. C., Haywood, J. M., Dunstone, N., Emanuel, K., Hawcroft, M. K., Hodges, K. I., & Jones, A. (2017). Impacts of hemispheric solar geoengineering on tropical cyclone frequency. *Nat. Commun.*, *8*(1), 1382. doi: 10.1038/s41467-017-01606-0

Jones, G. S., Stott, P. A., & Nikolaos, C. (2008). Human contribution to rapidly increasing frequency of very warm Northern Hemisphere summers. *J. Geophys. Res.*, *113*(D2). doi: 10.1029/2007JD008914

Jungclaus, J. H., Fischer, N., Haak, H., Lohmann, K., Marotzke, J., Matei, D., ... J., S. S. (2013). Characteristics of the ocean simulations in the Max Planck Institute Ocean Model (MPIOM) the ocean component of the MPI-Earth system model. *J. Adv. Model. Earth Syst.*, *5*(2), 422-446. doi: 10.1002/jame.20023

Keith, D., Parson, E., & Morgan, M. G. (2010). Research on global sun block needed now. *Nature*, *463*, 426-427.

Keith, D. W., & MacMartin, D. G. (2015). A temporary, moderate and responsive scenario for solar geoengineering. *Nature Clim. Change*, *5*, 201206. doi: https://doi.org/10.1038/nclimate2493

Keller, D. P., Feng, E. Y., & Oschlies, A. (2014). Potential climate engineering effectiveness and side effects during a high carbon dioxide-emission scenario. *Nat. Commun.*, *5*, 3304. doi: https://doi.org/10.1038/ncomms4304

Kosugi, T. (2013). Fail-safe solar radiation management geoengineering. *Mitig. Adapt. Strateg. Glob. Chang.*, *18*(8), 1141-1166. doi: 10.1007/s11027-012-9414-2

Kravitz, B., Alan, R., Olivier, B., Hauke, S., E., T. K., Georgiy, S., & Michael, S. (2011). The Geoengineering Model Intercomparison Project (GeoMIP). *Atmos. Sci. Lett.*, *12*(2), 162-167. doi: 10.1002/asl.316

Kug, J.-S., Jeong, J.-H., Jang, Y.-S., Kim, B.-M., Folland, C. K., Min, S.-K., & Son, S.-W. (2015). Two distinct influences of Arctic warming on cold winters over North America and East Asia. *Nature Geosci.*, *8*, 759-762.

Latham, J. (1990). Control of global warming? *Nature*, *347*(6291), 339-340. doi: 10.1038/347339b0

Latham, J. (2002). Amelioration of global warming by controlled enhancement of the albedo and longevity of low-level maritime clouds. *Atmos. Sci. Lett.*, *3*(2-4), 52-58. doi: 10.1006/asle.2002.0099

Latham, J., Bower, K., Choularton, T., Coe, H., Connolly, P., Cooper, G., ... Wood, R. (2012). Marine cloud brightening. *Phil. Trans. R. Soc. A*, *370*(1974), 4217–4262. doi: 10.1098/rsta.2012.0086

MacCracken, M. (2009). *Beyond Mitigation: Potential Options For Counter-Balancing The Climatic And Environmental Consequences Of The Rising Concentrations Of Greenhouse Gases*. The World Bank, Washington, DC. doi: 10.1596/1813-9450-4938

MacCracken, M. C. (2016). The rationale for accelerating regionally focused climate intervention research. *Earth's Future*, *4*(12), 649-657. doi: 10.1002/2016EF000450

MacCracken, M. C., Shin, H.-J., Caldeira, K., & Ban-Weiss, G. A. (2013). Climate response to imposed solar radiation reductions in high latitudes. *Earth Syst. Dyn.*, *4*(2), 301-315. doi: 10.5194/esd-4-301-2013

MacMartin, D. G., & Kravitz, B. (2019). Mission-driven research for stratospheric aerosol geoengineering. *Proc. Natl. Acad. Sci.*, *116*(4), 1089–1094. doi: 10.1073/pnas.1811022116

MacMartin, D. G., Kravitz, B., Tilmes, S., Richter, J. H., Mills, M. J., Lamarque, J.-F., ...

Vitt, F. (2017). The climate response to stratospheric aerosol geoengineering can be tailored using multiple injection locations. *J. Geophys. Res.*, *122*(23), 12,574-12,590. doi: 10.1002/2017JD026868

MacMartin, D. G., Wang, W., Kravitz, B., Tilmes, S., Richter, J. H., & Mills, M. J. (2019). Timescale for Detecting the Climate Response to Stratospheric Aerosol Geoengineering. *J. Geophys. Res.*, *124*(3), 1233-1247. doi: 10.1029/2018JD028906

Masunaga, H., & Bony, S. (2018). Radiative Invigoration of Tropical Convection by Preceding Cirrus Clouds. *J. Atmos. Sci*, *75*(4), 1327-1342. doi: 10.1175/JAS-D-17-0355.1

Matthews, H. D., & Caldeira, K. (2007). Transient climatecarbon simulations of planetary geoengineering. *Proc. Natl. Acad. Sci. USA.*, *104*(24), 9949-9954. doi: 10.1073/pnas.0700419104

McComiskey, A., & Feingold, G. (2008). Quantifying error in the radiative forcing of the first aerosol indirect effect. *Geophys. Res. Lett.*, *35*(2). doi: 10.1029/2007GL032667

Meehl, G. A., & Tebaldi, C. (2004). More Intense, More Frequent, and Longer Lasting Heat Waves in the 21st Century. *Science*, *305*(5686), 994–997. doi: 10.1126/science.1098704

Mitchell, D. L., & Finnegan, W. (2009). Modification of cirrus clouds to reduce global warming. *Environ. Res. Lett.*, *4*(4), 045102. doi: doi:10.1088/1748-9326/4/4/045102

Mitchell, D. L., Philip, R., Dorothea, I., Greg, M., & Timo, N. (2008). Impact of small ice crystal assumptions on ice sedimentation rates in cirrus clouds and GCM simulations. *Geophys. Res. Lett.*, *35*(9). doi: 10.1029/2008GL033552

Moreno-Cruz, J. B., Ricke, K. L., & Keith, D. W. (2012). A simple model to account for regional inequalities in the effectiveness of solar radiation management. *Clim. Chang.*, *110*(3), 649-668. doi: https://doi.org/10.1007/s10584-011-0103-z

Muri, H., Kristjánsson, J. E., Storelvmo, T., & Pfeffer, M. A. (2014). The climatic effects of modifying cirrus clouds in a climate engineering framework. *J. Geophys. Res.*, *119*(7), 4174–4191. doi: 10.1002/2013JD021063

Parker, A., & Irvine, P. J. (2018). The Risk of Termination Shock From Solar Geoengineering. *Earth's Future*, *6*(3), 456-467. doi: 10.1002/2017EF000735

Preston, C. J. (2013). Ethics and geoengineering: reviewing the moral issues raised by solar radiation management and carbon dioxide removal. *WIREs Clim. Change*, *4*(1), 23-37. doi: 10.1002/wcc.198

Quaas, J., Quaas, M. F., Boucher, O., & Rickels, W. (2016). Regional climate engineering by radiation management: Prerequisites and prospects. *Earth's Future*, *4*(12), 618–625. doi: 10.1002/2016EF000440

Quaas, M. F., Quaas, J., Rickels, W., & Boucher, O. (2017). Are there reasons against open-ended research into solar radiation management? A model of intergenerational decision-making under uncertainty. *J. Environ. Econ. Manag.*, *84*, 1 - 17. doi: https://doi.org/10.1016/j.jeem.2017.02.002

Rahm, D. (2018). Geoengineering Climate Change Solutions: Public Policy issues for National and Global Governance. *Humanities and Social Sciences Review*, *08*(02), 139-148.

Robock, A., MacMartin, D. G., Duren, R., & Christensen, M. W. (2013). Studying geoengineering with natural and anthropogenic analogs. *Clim. Chang.*, *121*(3), 445–458. doi: 10.1007/s10584-013-0777-5

Robock, A., Oman, L., & Stenchikov, G. L. (2008). Regional climate responses to geoengineering with tropical and Arctic $SO_2$ injections. *J. Geophys. Res.*, *113*(D16). (D16101) doi: 10.1029/2008JD010050

Sillmann, J., Kharin, V. V., Zhang, X., Zwiers, F. W., & Bronaugh, D. (2013). Climate extremes indices in the CMIP5 multimodel ensemble: Part 1. Model evaluation in the present climate. *J. Geophys. Res.*, *118*(4), 1716-1733. doi: 10.1002/jgrd.50203

Stevens, B., Giorgetta, M., Esch, M., Mauritsen, T., Crueger, T., Rast, S., ... Roeckner, E. (2013). Atmospheric component of the MPI-M Earth System Model: ECHAM6. *J. Adv. Model. Earth Syst.*, *5*(2), 146-172. doi: 10.1002/jame.20015

Stjern, C. W., Muri, H., Ahlm, L., Boucher, O., Cole, J. N. S., Ji, D., ... Kristjánsson,

J. E. (2018). Response to marine cloud brightening in a multi-model ensemble. *Atmos. Chem. Phys.*, *18*(2), 621–634. doi: 10.5194/acp-18-621-2018

Storelvmo, T., Boos, W. R., & Herger, N. (2014). Cirrus cloud seeding: a climate engineering mechanism with reduced side effects? *Phil. Trans. R. Soc. A*, *372*(2031). doi: 10.1098/rsta.2014.0116

Storelvmo, T., Kristjansson, J. E., Muri, H., Pfeffer, M., Barahona, D., & Nenes, A. (2013). Cirrus cloud seeding has potential to cool climate. *Geophys. Res. Lett.*, *40*(1), 178–182. doi: 10.1029/2012GL054201

Sugiyama, M., Arino, Y., Kosugi, T., Kurosawa, A., & Watanabe, S. (2018). Next steps in geoengineering scenario research: limited deployment scenarios and beyond. *Climate Policy*, *18*(6), 681-689. doi: 10.1080/14693062.2017.1323721

Sun, Y., Zhang, X., Zwiers, F. W., Song, L., Wan, H., Hu, T., ... Ren, G. (2014). Rapid increase in the risk of extreme summer heat in Eastern China. *Nature Clim. Change*, *4*, 10821085. doi: https://doi.org/10.1038/nclimate2410

Tilmes, S., Fasullo, J., Lamarque, J.-F., Marsh, D. R., Mills, M., Alterskjr, K., ... Watanabe, S. (2013). The hydrological impact of geoengineering in the Geoengineering Model Intercomparison Project (GeoMIP). *J. Geophys. Res.*, *118*(19), 11,036-11,058. doi: 10.1002/jgrd.50868

Tilmes, S., Garcia, R. R., Kinnison, D. E., Gettelman, A., & Rasch, P. J. (2009). Impact of geoengineered aerosols on the troposphere and stratosphere. *J. Geophys. Res.*, *114*(D12). (D12305) doi: 10.1029/2008JD011420

Tilmes, S., Jahn, A., Kay, J. E., Holland, M., & Lamarque, J.-F. (2014). Can regional climate engineering save the summer Arctic sea ice? *Geophys. Res. Lett.*, *41*(3), 880–885. doi: 10.1002/2013GL058731

Tilmes, S., Richter, J. H., Kravitz, B., MacMartin, D. G., Mills, M. J., Simpson, I. R., ... Ghosh, S. (2018). CESM1(WACCM) Stratospheric Aerosol Geoengineering Large Ensemble Project. *Bull. Amer. Meteor. Soc.*, *99*(11), 2361-2371. doi: 10.1175/BAMS-D-17-0267.1

Twomey, S. (1977). The Influence of Pollution on the Shortwave Albedo of Clouds. *J. Atmos. Sci.*, *34*(7), 1149-1152. doi: 10.1175/1520-0469(1977)034⟨1149:TIOPOT⟩2.0.CO;2

UNFCCC. (2015). Adoption of the Paris agreement, proposal by the president. Retrieved from `http://unfccc.int/resource/docs/2015/cop21/eng/l09r01.pdf`

Wang, M., Yan, X., Liu, J., & Zhang, X. (2013). The contribution of urbanization to recent extreme heat events and a potential mitigation strategy in the Beijing–Tianjin–Hebei metropolitan area. *Theor. Appl. Climatol.*, *114*(3), 407–416. doi: 10.1007/s00704-013-0852-x

Welch, B. L. (1947). The Generalization of 'Student's' Problem When Several Different Population Variances Are Involved. *Biometrika*, *34*(1/2), 28-35. doi: 10.2307/2332510

Wigley, T. M. L. (2006). A Combined Mitigation/Geoengineering Approach to Climate Stabilization. *Science*, *314*(5798), 452–454. doi: 10.1126/science.1131728

Wigley, T. M. L., & Raper, S. C. B. (2001). Interpretation of High Projections for Global-Mean Warming. *Science*, *293*(5529), 451–454. doi: 10.1126/science.1061604

Wolf, J., Adger, W. N., Lorenzoni, I., Abrahamson, V., & Raine, R. (2010). Social capital, individual responses to heat waves and climate change adaptation: An empirical study of two UK cities. *Glob. Environ. Change*, *20*(1), 44 - 52. doi: https://doi.org/10.1016/j.gloenvcha.2009.09.004

Wood, R., & Ackerman, T. P. (2013). Defining success and limits of field experiments to test geoengineering by marine cloud brightening. *Climatic Chang.*, *121*(3), 459–472. doi: 10.1007/s10584-013-0932-z

**Table 1.** An overview of the year, beginning (10 days before HW) and end date (7 days after HW) of the intermittent RRM experiment.

| No | Year No | Begin Date | End Date | HW length (days) |
|---|---|---|---|---|
| 1. | Y02 | 1851-07-01 | 1851-08-10 | 23 |
| 2. | Y04 | 1853-07-19 | 1853-08-10 | 06 |
| 3. | Y05 | 1854-07-12 | 1854-08-09 | 04 |
| 4. | Y10 | 1859-07-18 | 1859-08-14 | 11 |
| 5. | Y11 | 1860-06-24 | 1860-07-17 | 07 |
| 6. | Y12 | 1861-07-09 | 1861-08-19 | 06 |
| 7. | Y14 | 1863-06-21 | 1863-08-03 | 04 |
| 8. | Y18 | 1867-06-25 | 1867-07-29 | 09 |
| 9. | Y19 | 1868-08-06 | 1868-08-28 | 06 |
| 10. | Y21 | 1870-07-09 | 1870-08-22 | 28 |
| 11. | Y24 | 1873-07-15 | 1873-08-03 | 07 |
| 12. | Y24 | 1874-07-03 | 1874-08-11 | 23 |
| 13. | Y25 | 1875-07-20 | 1875-08-20 | 15 |
| 14. | Y27 | 1877-06-22 | 1877-08-05 | 28 |
| 15. | Y29 | 1878-06-24 | 1879-07-24 | 14 |
| 16. | Y30 | 1879-07-15 | 1879-08-21 | 21 |

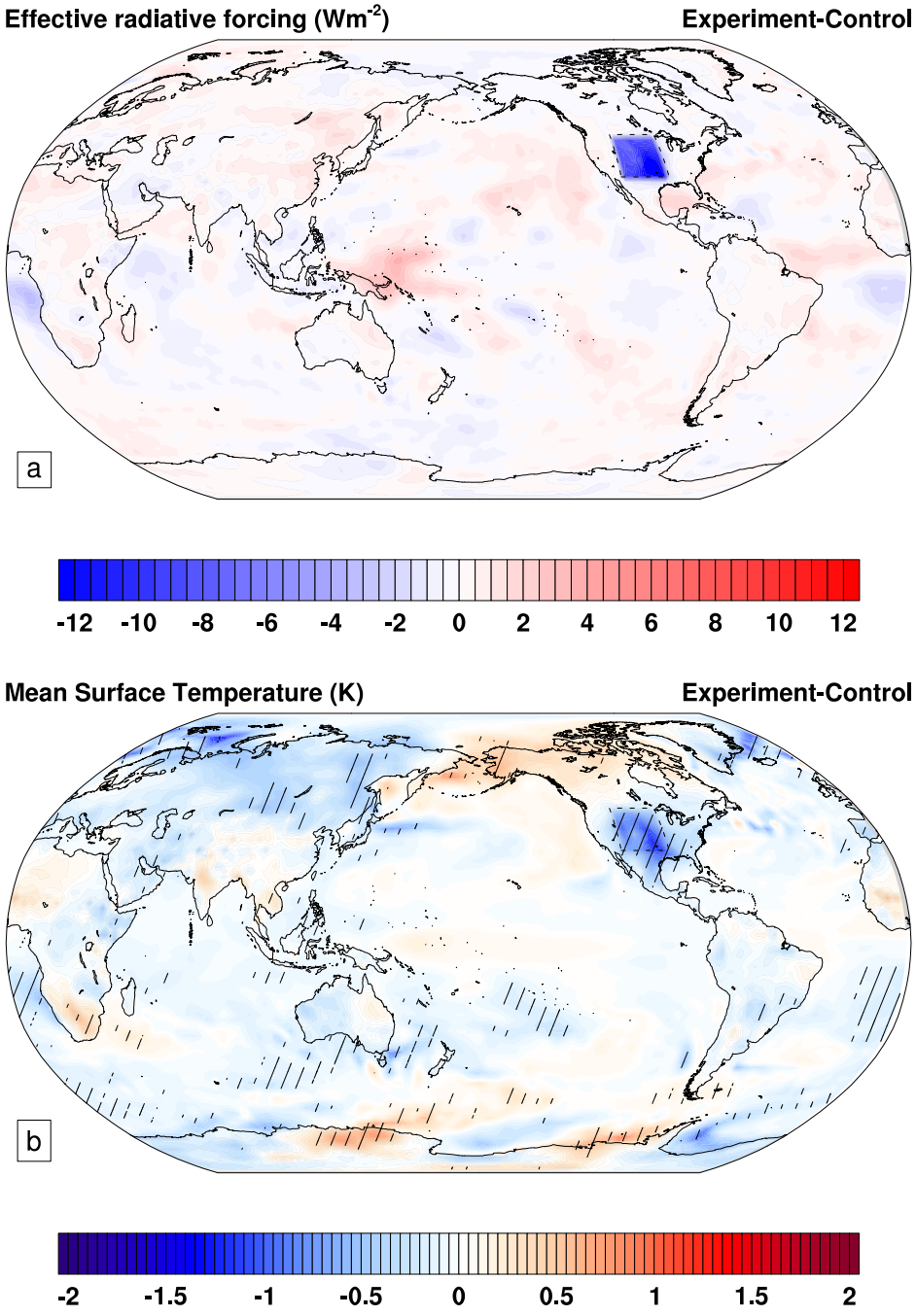


**Figure 1.** **(a)** Effective radiative forcing (ERF, W m $^{-2}$) at the top of the atmosphere and, **(b)** near-surface air temperature (SAT, K) change as 30-year average (experiment - control), ensemble average differences between the sustained RRM and control simulations. Hatched areas are grid cells where the changes are statistically significant at the 90% level according to a *t*-test.

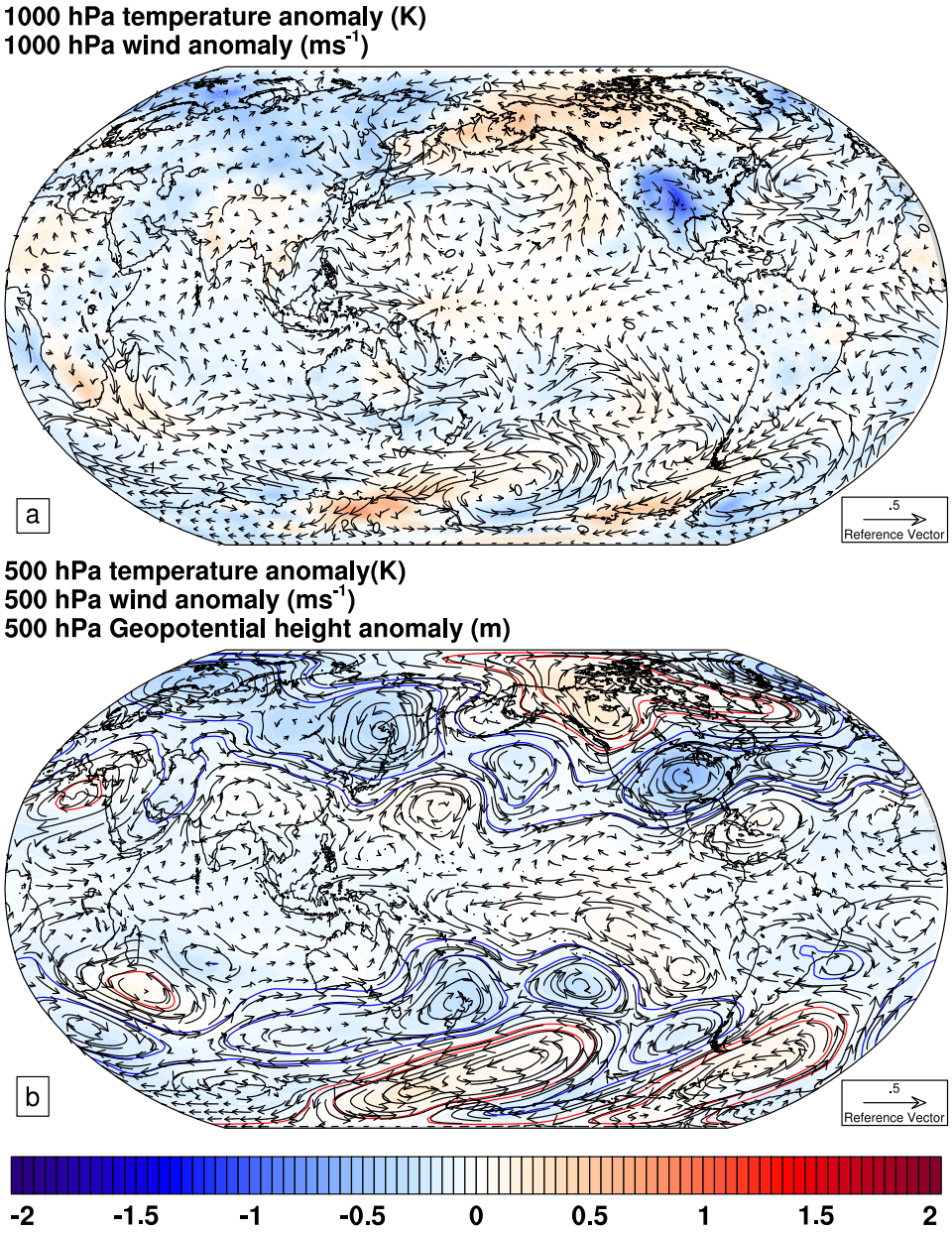


**Figure 2.** As Fig. 1 but for **(a)** 1000 hPa air temperature (K) and wind vector ($\mathrm{m\,s^{-1}}$) **(b)** 500 hPa air temperature (color shades), wind vector ($\mathrm{m\,s^{-1}}$) and geopotential height (m, contours from −4 to 4 by 2), and wind vector anomaly.

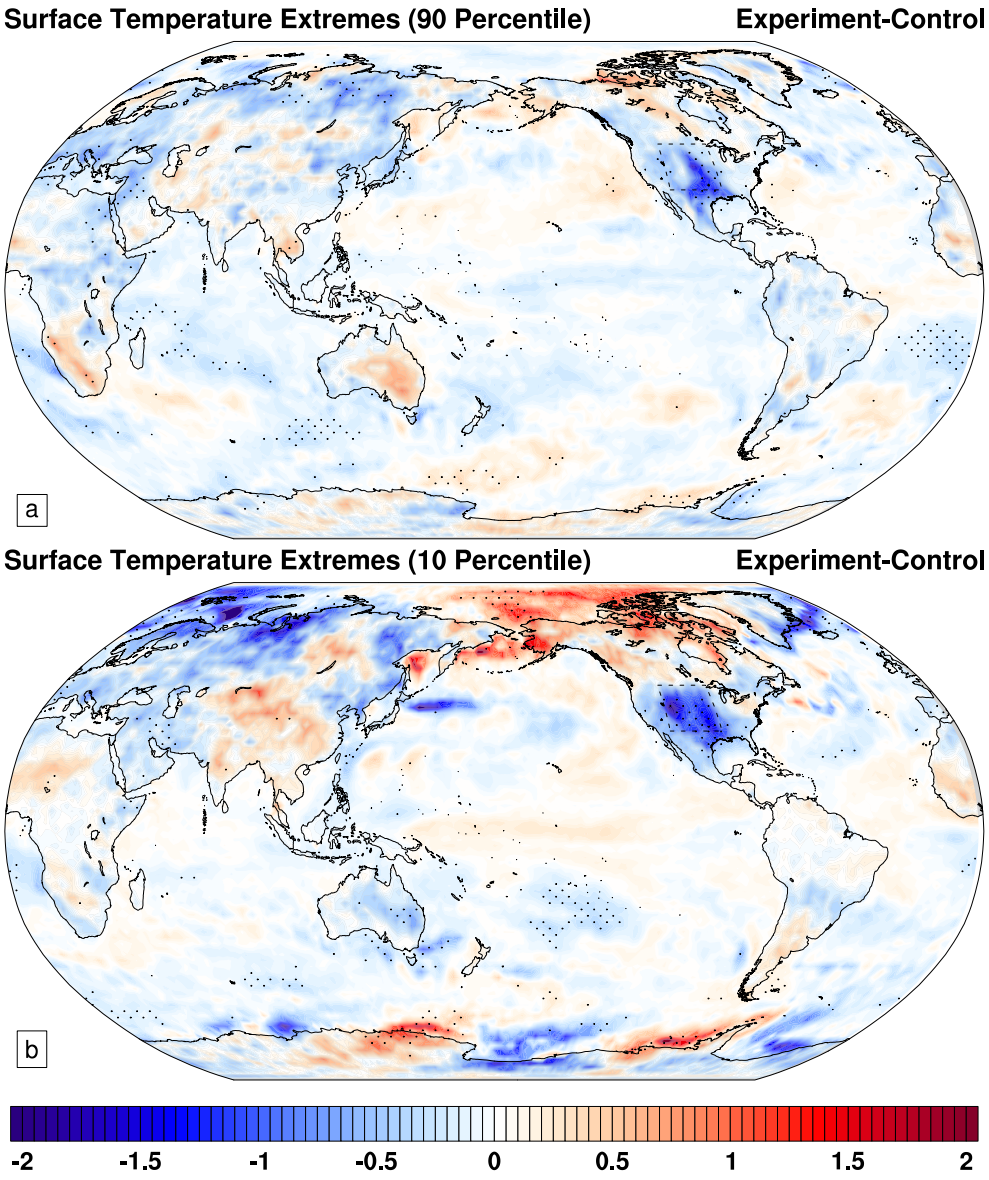


**Figure 3.** As Fig. 1 but for the change in **(a)** top decile ($90^{th}$ percentile) and, **(b)** the bottom decile ($10^{th}$ percentile) of the temporal distribution of surface temperature. A 90% significance level is shown as dotted.

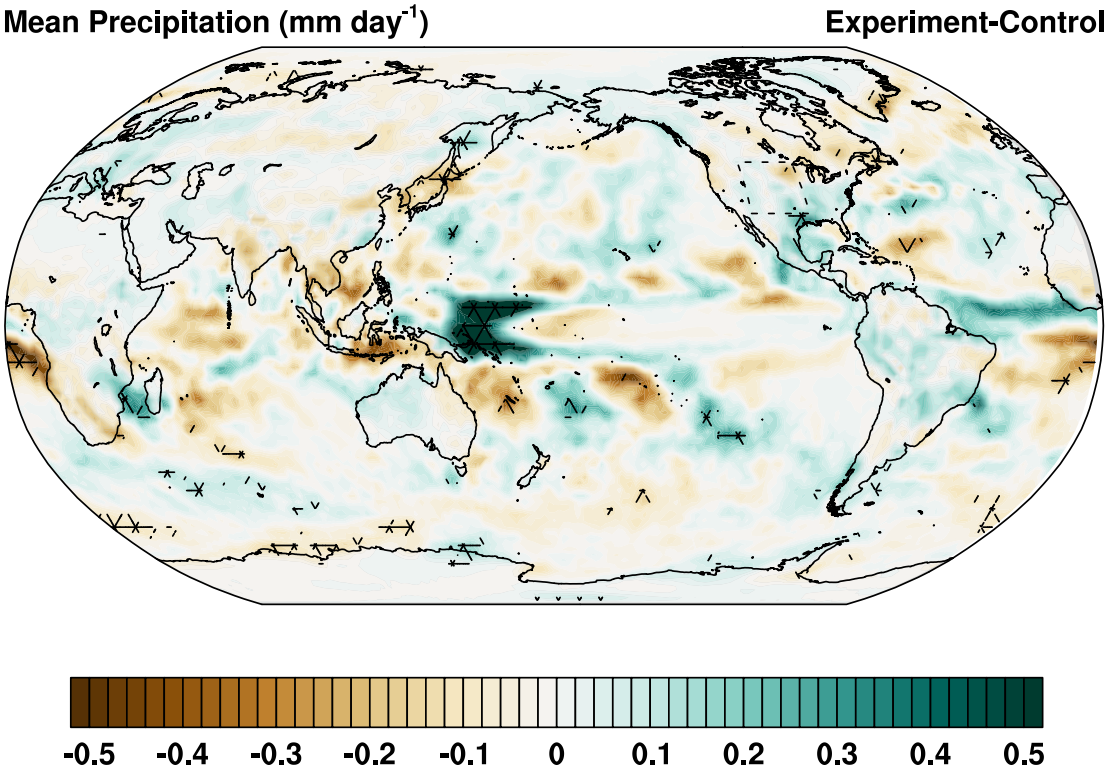


**Figure 4.** As Fig. 1 but for change in total precipitation (mm/day).

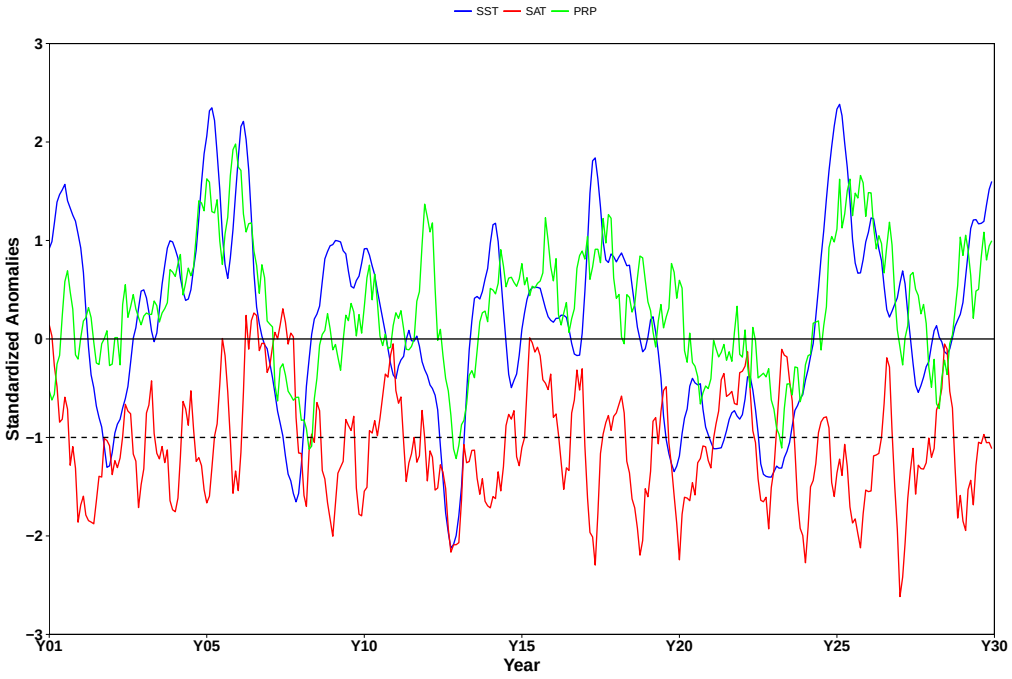


**Figure 5.** Time evolution of the standardized anomalies of surface air temperature (SAT) in the RRM region (red line), the sea surface temperature (SST) in the Niño3.4 region (5° S to 5° N, 120° W to 170° W, blue line), and total precipitation in the east Pacific region (0° S to −10° S, 148° E to 180° E, green line). The standardized anomalies are averaged for the respective regions. The dashed line shows the SAT at −1.0 in the RRM region, which differentiates the strong and weak cooling scenarios.

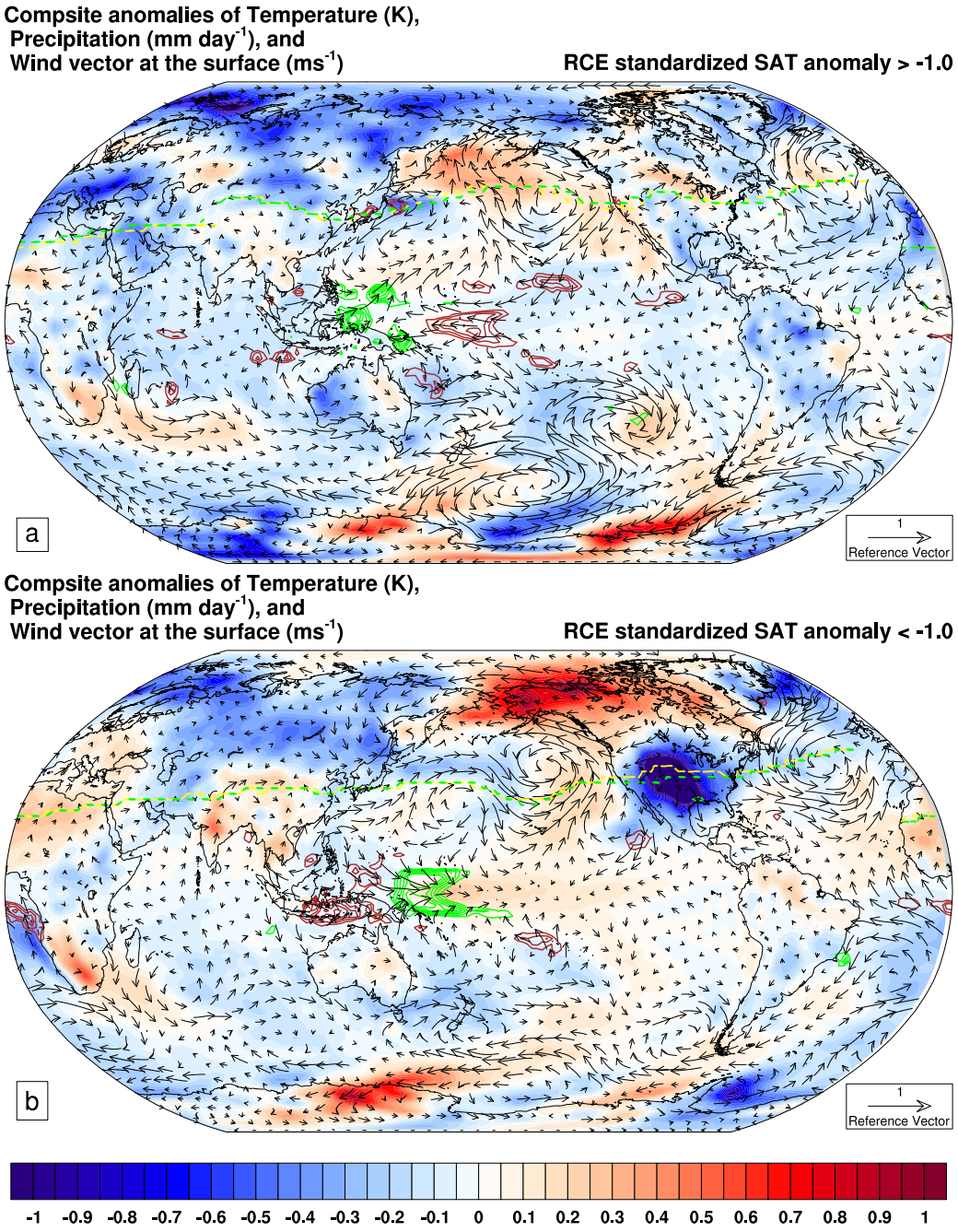


**Figure 6.** **(a)** Composite anomalies relative to the control simulation of surface air temperature (SAT in K, color scale), precipitation (mm/day, green contours are for positive and brown contours for negative anomalies, contours from −2.0 to 2.0 with a spacing of 0.25), and wind vector ($\mathrm{m\,s^{-1}}$) at the surface for conditions in which the standardized SAT in the RRM region is greater than −1.0 K, **(b)** same as (a) but for conditions in which the standardized SAT in the RRM region is smaller than −1.0 K. The green (experiment) and yellow (control) dotted lines represent the core of the jet stream ($\mathrm{m\,s^{-1}}$, max. zonal wind between 300 and 200 hPa).

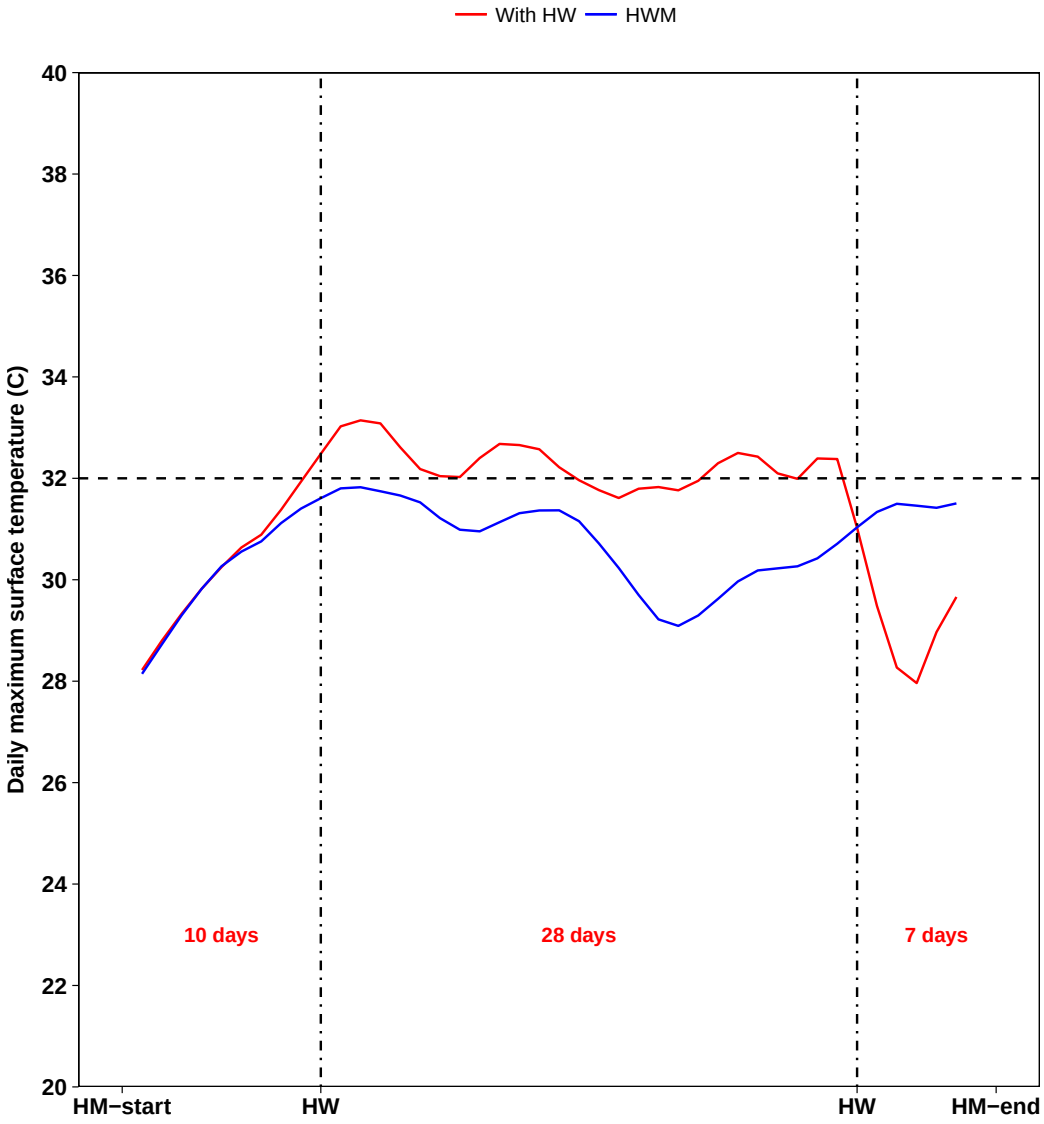


**Figure 7.** Time evolution of the RRM area-averaged daily maximum surface air temperature (°C) for a HW condition (red line, dark blue simulation with HWs in Fig. S2), and the corresponding ensemble mean HW mitigation (blue line), with a heat wave duration in the control of 28 days (Refer Fig. S2 for detailed description of intermittent RRM experiment). The horizontal dotted line at 32° C represents the threshold of HWs (Refer Fig. S6 for the time evolution of the SAT in all individual identified and suppressed HWs).

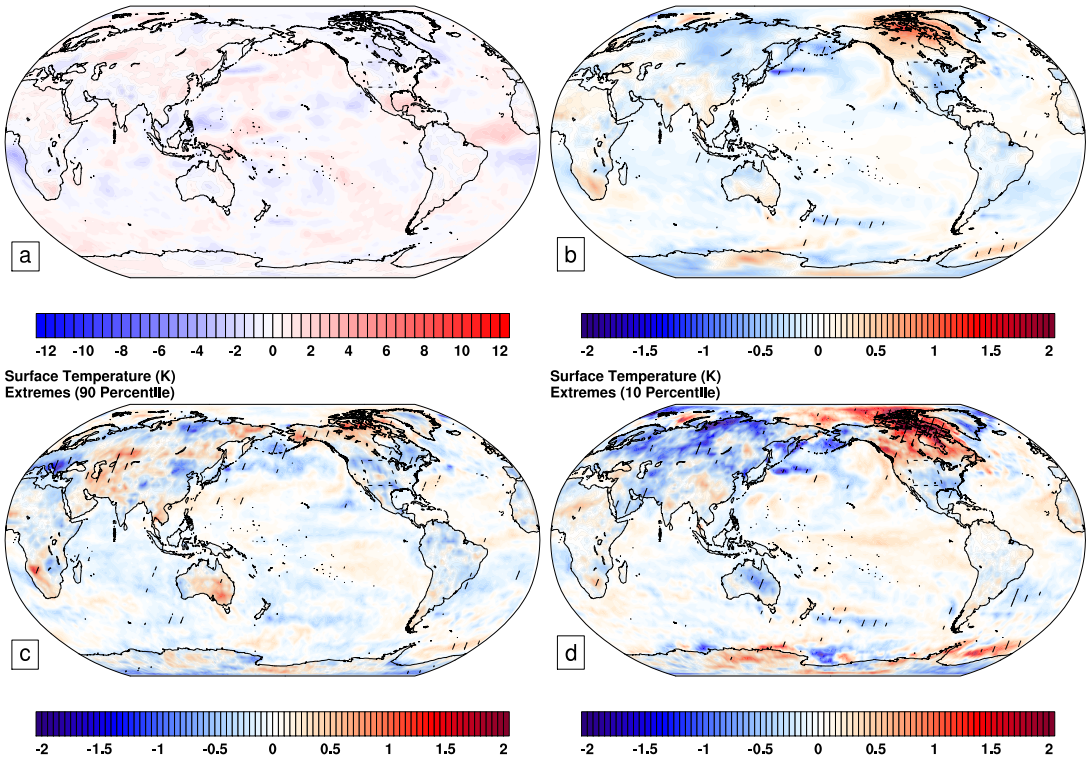


**Figure 8.** For intermittent RRM simulation **(a)** Effective radiative forcing (ERF, $\mathrm{W\,m^{-2}}$) at the top of the atmosphere, **(b)** mean change in near-surface air temperature (SAT, K) response. Hatched areas in (b) are grid cells where significant at the 90% level by the $t$-test. Change in **(c)** top decile ($90^{th}$ percentile) **(d)** bottom decile ($10^{th}$ percentile) of temperature distribution. The difference shown are thirty year ensemble ensemble average between the HW suppression and control simulations (In Fig. S2, the light blue lines indicate control simulation and the dashed red line in the intermittent simulation represents the ensemble part). Hatched areas in (c) and (d) are grid cells where significant at the 90% level by the $t$-test.

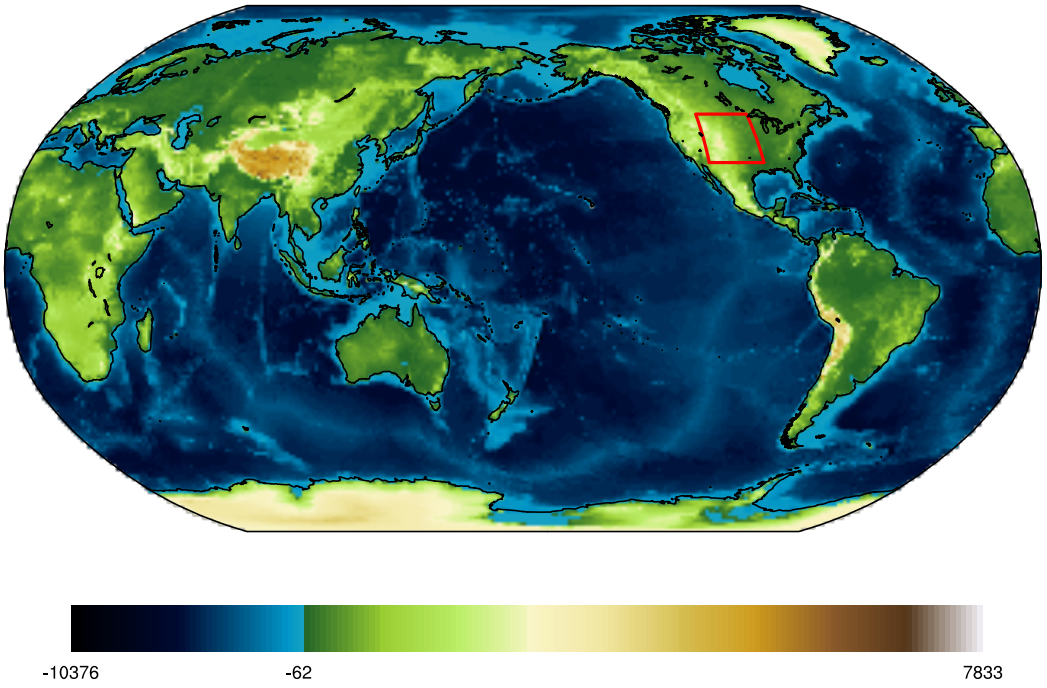


**Figure S1.** Geographical location of regional radiation management (RRM, 32.5° N to 47.5° N, 112.0° W to 92.0°W). The blue and the green/brown colors indicate the ocean and the orography, respectively [data source: Hastings et al. (1999)].

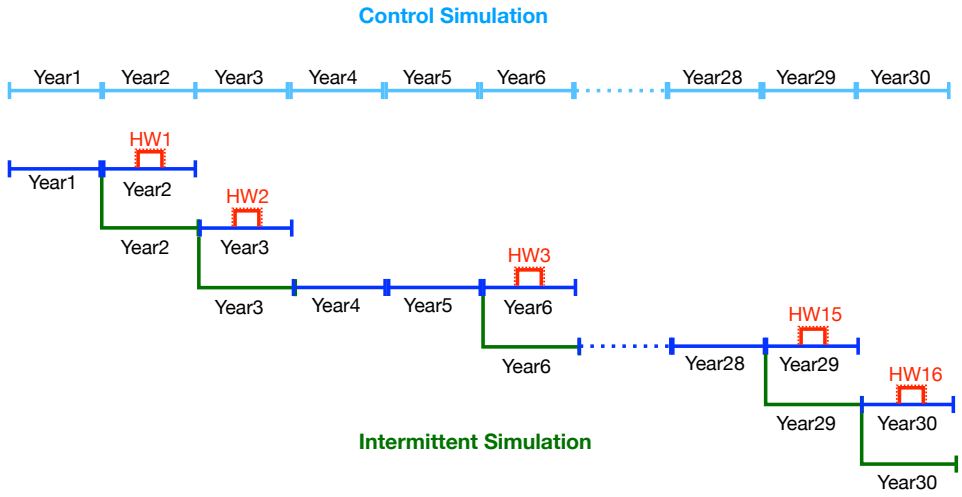


**Figure S2.** Schematic representation of the control and intermittent simulation. The long term consequences of HW suppression is estimated from the thirty-year mean control and intermittent simulation. The light blue lines indicate control simulation, dark blue lines indicate year without HWs, dark blue lines with red peaks indicate year with HWs and the green lines indicate year with HW suppression. The dashed red line in the intermittent simulation represents the ensemble part.

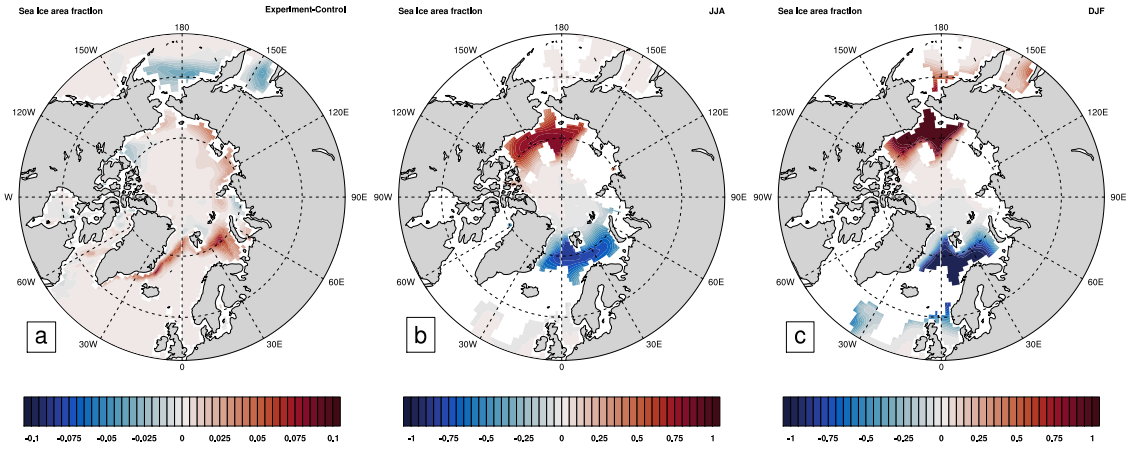


**Figure S3.** Change in sea ice area fraction in the Northern Hemisphere due to sustained RRM **(a)** in annual mean **(b)** during summer (JJA) and **(c)** during winter (DJF).

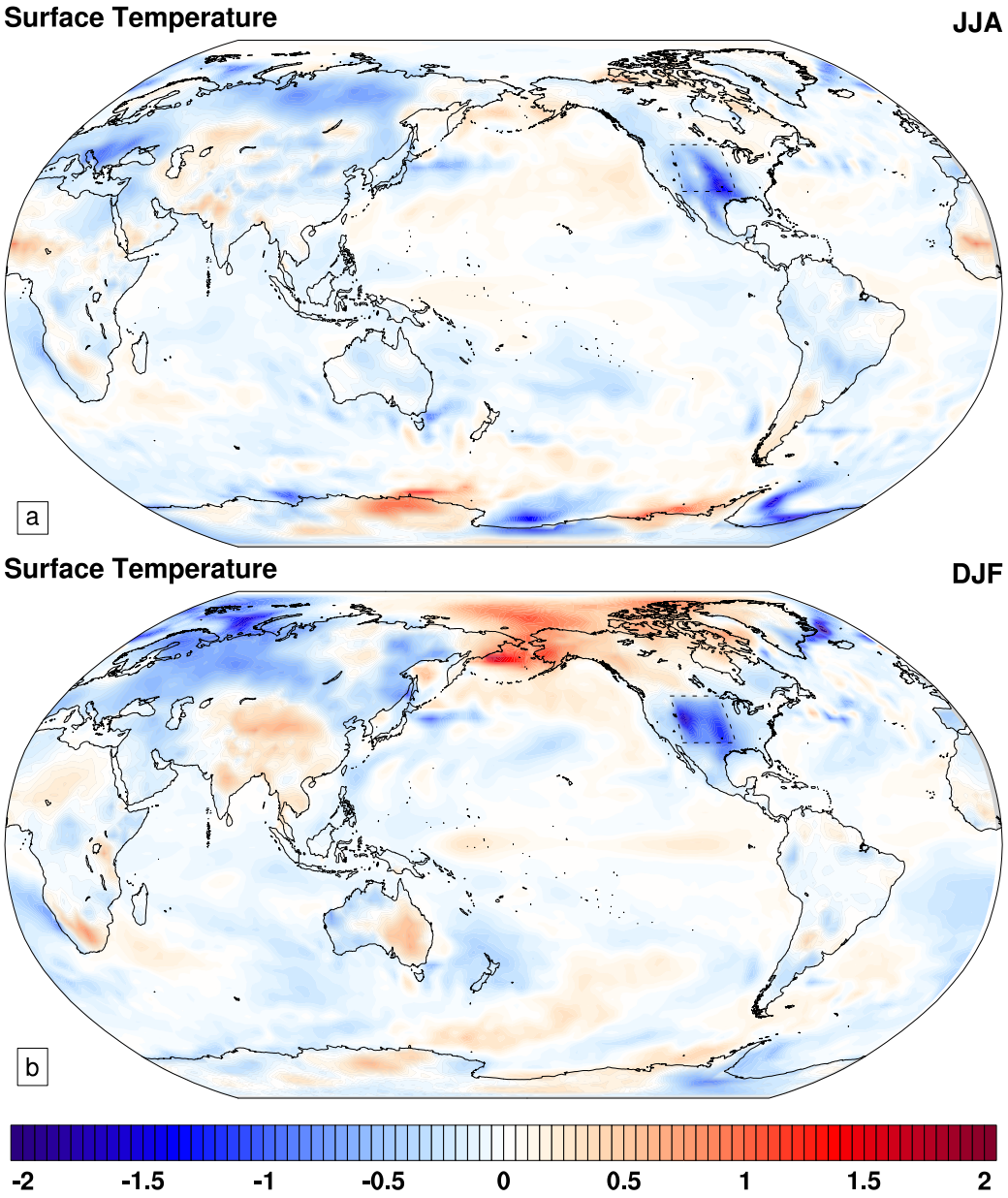


**Figure S4.** For sustained RRM simulation, seasonal change in SAT **(a)** for the summer season (JJA) and **(b)** for the winter season (DJF).

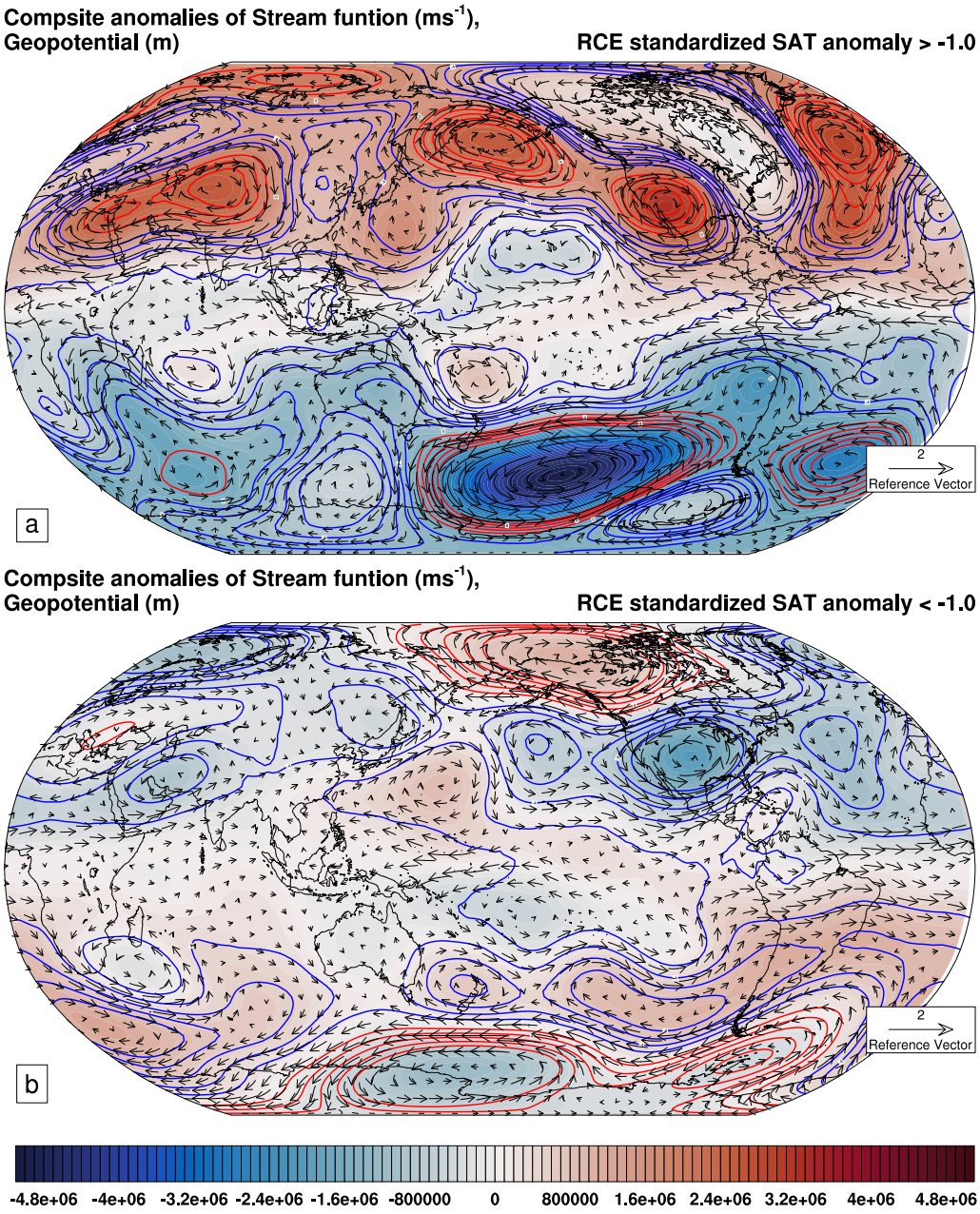


**Figure S5.** For sustained RRM simulation, **(a)** composite anomalies of the stream function ($\mathrm{m\,s^{-1}}$, shaded), wind vector ($\mathrm{m\,s^{-1}}$) and, geopotential height (m, red contours are for positive and blue contours for negative anomalies) at 200 hPa for conditions in which the standardized SAT in the RRM region greater than $-1.0$ K, and **(b)** as (a), but for conditions in which the standardized SAT in the RRM region less than $-1.0$ K.

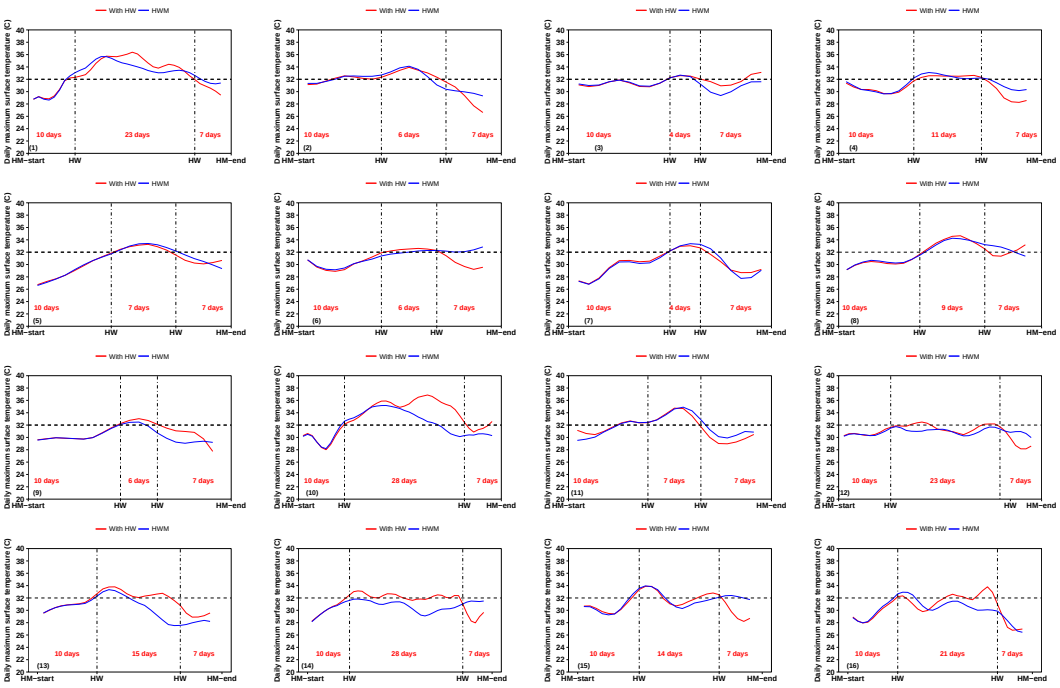


**Figure S6.** Time evolution of the area-averaged daily maximum surface air temperature (°C) for the simulation with HW (red curve) and with HW suppression (blue curve).